Spatiotemporal variability of extreme precipitation events and associated atmospheric processes over Dronning Maud Land, East Antarctica

*Sibin Simon** [1,2], *John Turner*[3], *Meloth Thamban*[1], *Jonathan D. Wille*[4,5], *Pranab Deb*[6]

[1]National Centre for Polar and Oceans Research, Goa, India

[2]School of Earth Ocean and Atmospheric Sciences, Goa University, Goa, India.

[3]Cambridge, UK

[4]Institut des Géosciences de l'Environnement, CNRS/UGA, Saint Martin d'Hères, France

[5]Institute for Atmospheric and Climate Science, ETH Zurich, Zurich, Switzerland

[6]Centre for Ocean, River, Atmosphere and Land Sciences, Indian Institute of Technology Kharagpur, Kharagpur, West Bengal, India

*Corresponding author: Sibin Simon (sibin@ncpor.res.in)

Key Points:

- Spatial distribution of extreme precipitation events is linked to the complex orography of the Dronning Maud Land sector of Antarctica.
- Interannual variability of extreme precipitation events is controlled by blocking high-pressure systems north of the location.
- Increased moisture content and poleward winds in the south Atlantic Ocean contributed to increasing trend in high-precipitating days.

Abstract

We investigate the spatial and temporal variability of extreme precipitation events (EPEs) in the Dronning Maud Land (DML) sector of Antarctica using high-resolution ECMWF ERA5 reanalysis data. This study examines the spatial occurrence of EPEs across DML, focusing particularly on six locations spanning the coastal and interior parts of the area. The largest snowfall amounts are usually found on eastward-facing slopes in the coastal zone. EPEs occur predominantly in north-easterly to easterly flows, leading to enhanced precipitation on the windward side of the orographic features with a steep gradient. Wind during EPEs was found to be more directionally consistent in the coastal area than in the interior. An east-west couplet of a mid-tropospheric ridge and low-pressure center is essential for steering warm moist maritime airmasses into the DML region before EPEs. Approximately 40% of EPEs result from atmospheric rivers (ARs), narrow bands of moist air originating at subtropical latitudes, which provide the greatest daily precipitation amounts. From 1979 to 2018, much of the DML experienced a statistically significant ($p < 0.05$) increase in the number of EPEs per year, along with increased precipitation from the EPEs. These trends were associated with significant changes in moisture availability and poleward meridional winds in the Atlantic sector of the Southern Ocean. The inter-annual variability in the number of EPEs is primarily dictated by regional atmospheric variability, while the influence of the Southern Oscillation Index and Southern Annular Mode is limited.

Plain Language Summary

Extreme precipitation events are severe weather conditions that cause unusually large amounts of rain or snow, leading to natural disasters. In Antarctica, a substantial proportion of precipitation comes from these high-magnitude precipitation events and they control the year-to-year variability in annual total precipitation, particularly in the coastal region. These events have a significant impact on different aspects of the Antarctic climate system and can make anomalous changes in meteorological parameters. We

investigate the influence of these extreme events over the Dronning Maud Land (DML) region of Antarctica and show that the terrain of the region plays a significant role in their distribution. We found that most of these events are caused by the combined influence of low-pressure cyclones and anticyclones, which aids moisture transport to the region. The strong, long, and narrow bands of moisture transport called atmospheric rivers (ARs), from far north of the region, are involved in over 40% of EPEs. Over recent decades, there has been an increasing trend in the occurrence of these high precipitating days, which is associated with increased moisture content and favorable winds in the South Atlantic sector of the Southern Ocean, north of Antarctica.

1. Introduction

Most of the Earth's ice is located in the Antarctic ice sheet, which is susceptible to climate change and the mass loss that results in sea level change (Church et al., 2001; Pritchard et al., 2012). The balance between precipitation input, net evaporation, drifting snow, and melt-water runoff determines the Antarctic continent's surface mass balance (Bromwich, 1988; Rignot et al., 2019). Therefore, precipitation over Antarctica is a crucial factor affecting the ice sheet's dynamics and growth, which mitigates sea level rise (Lenaerts et al., 2013; Medley & Thomas, 2019). The projected increase in Antarctic precipitation under increasing greenhouse gas concentration scenarios during the twenty-first century (Genthon et al., 2009) highlights the significance of understanding the processes involved in precipitation formation and its spatial, and temporal distribution in Antarctica (Souverijns et al., 2018).

The frequency and magnitude of precipitation over Antarctica differ substantially from coast to inland, with extremely small quantities of clear sky precipitation falling from thin, isolated clouds or a seemingly clear sky in inland locations. In contrast, snowfall near the coast is episodic and often consists of large precipitation amounts (Bromwich, 1988). These infrequent heavy precipitation episodes have high seasonal and interannual variability and contribute significantly to the annual total of precipitation in

just a few days (Gorodetskaya et al., 2014; Turner et al., 2019). Extreme Precipitation Events (EPEs) are infrequent and often defined as days above a particular threshold calculated from the long-term time series of precipitation (Schlosser, Manning, et al., 2010; Yu et al., 2018). The isotope records from ice cores are affected by the seasonality and intermittent nature of these occurrences (Münch et al., 2017; Münch & Laepple, 2018; Zuhr et al., 2021). Thus, an improved understanding of the variability and seasonality of EPEs, the atmospheric processes underlying them, moisture transport and mechanism, and changes in atmospheric parameters at the deposition location, are required for improved reconstruction of historical climatic records from ice cores (Noone et al., 1999; Turner et al., 2019). The synoptic patterns and features of high precipitation events have been studied for different regions of Antarctica, such as the coastal region of the Antarctic Peninsula (González-Herrero et al., 2023; Turner et al., 1995, 1997) , Amundsen Sea Embayment (Swetha Chittella et al., 2022), Ross Sea (Markle et al., 2012; Sinclair et al., 2010), Prydz Bay region (Yu et al., 2018) and in the interior, such as Dome C and Kohnen Station in Dronning Maud Land (DML) (Birnbaum et al., 2006; Schlosser, Manning, et al., 2010).

The DML is the region between 20°W and 45°E in East Antarctica, situated mainly south of the Atlantic Ocean, and is characterised by steep orography, particularly near the coast (Rotschky et al., 2007). Snow distribution in DML is strongly related to orographic features and wind-driven sublimation and redistribution on the grounded ice sheet (Reijmer et al., 2004; Thiery et al., 2012). Coastal DML is prone to intermittent and intense EPEs, which significantly contribute to more than half (50%) of annual total precipitation in a few days each year (Reijmer & Broeke, 2003; Turner et al., 2019). Due to the importance of DML as a location for numerous ice core drilling programmes (such as the European Project for Ice Coring in Antarctica (EPICA)), several studies have examined the pattern and distribution of precipitation over the region (Birnbaum et al., 2006; Noone et al., 1999; Schlosser, Powers, et al., 2010; Welker et al., 2014). Some studies (Gorodetskaya et al., 2014; Lenaerts et al., 2013; Schlosser et al., 2016) examined the characteristics of anomalous high precipitation years, while others (Noone et al.,

1999; Schlosser, Powers, et al., 2010) studied the detailed occurrence of these events using case studies based on available high-resolution model and reanalysis data. In terms of the availability of in-situ observations, the majority of the research spans just a few years (Birnbaum et al., 2006; Reijmer & Broeke, 2003; Schlosser, Manning, et al., 2010), and only a few studies (Welker et al., 2014) used a climatological approach to examine high precipitation episodes. The anomalous nature of the winds and temperature during EPEs have been reported in several studies (Reijmer & Broeke, 2001; Servettaz et al., 2020). The dispersal of precipitated snow, also known as drifting or blowing snow, is primarily influenced by the strong winds during precipitation episodes (Bromwich et al., 2004; Lenaerts & van den Broeke, 2012). The region's orography substantially influences the wind direction and speed, affecting snow distribution during precipitation events (Lenaerts et al., 2012). During EPEs, the surface temperature also exhibits unusual shifts and rapid fluctuations (Turner et al., 2022), which is due to the changes in longwave radiation flux driven by cloud cover, atmospheric blocking episodes, and warm airmasses moving over high orography (Hirasawa et al., 2000; Schlosser, Manning, et al., 2010; Turner et al., 2021).

Recent studies have shown that atmospheric rivers (ARs), which are long, narrow bands of intense horizontal water vapour transport, can bring significant amounts of moisture to DML and are responsible for 20–40% of the region's annual precipitation total (Gorodetskaya et al., 2014; Wille et al., 2021). These bands frequently originate in the tropics or subtropics and then extend southward, carrying large quantities of water vapour (Ralph et al., 2004; Zhu & Newell, 1998). Due to the significant intrusions of warm moist air, ARs landfalling in coastal Antarctica contribute to heavy snowfall, accounting for about 70% to 80% of the surface mass balance (SMB) and also affect melt processes in the ice sheet (Bozkurt et al., 2018; Gorodetskaya et al., 2014; Wille et al., 2019). Wille et al. (2021), in their Antarctic-wide climatological analysis of ARs from 1980-2018, showed a significant increase in the number of ARs across DML. During a two-year period from 2009-2011, exceptional AR activity

accounted for 74-80% of total accumulated snowfall around Princess Elizabeth Station in DML and caused a strongly positive regional SMB signal (Gorodetskaya et al., 2014). In addition, this region is more prone to short-lived EPE events than precipitation generated by cyclonic activity (Turner et al., 2019; Wille et al., 2021). The expected warming climate will lead to an increase in the atmospheric saturation vapour pressure and moisture, and ARs will have a more significant snowfall potential over coastal Antarctica with local orographic interaction (Dalaiden et al., 2020; Wille et al., 2021).

In this study, we use high-resolution reanalysis data from European Centre for Medium-range Weather Forecasts (ECMWF) to examine the spatial and temporal variability of EPEs over the DML region for the 40-year period (1979-2018). Since DML is an area with complex orography characterised by steep mountains and nunataks (Rotschky et al., 2007), it is essential to examine how the orography influences the occurrence and distribution of EPEs in the area. This study examines the spatial changes in 2-m temperature and 10-m wind during EPEs and compares them with climatological values. To further understand the spatial variability of EPEs in the coastal and inland regions, we focus on six locations (see Table 1) that represent both low-elevation coastal locations (altitude < 2000 m) and the high-altitude interior, East Antarctic Plateau (EAP) region (altitude > 2000 m). The latter are also sites of high-resolution ice core records and are available for future data-proxy comparison. We analyse the interannual and seasonal variability of EPEs occurrence, the factors controlling this variability, and the synoptic environment in which they occur. We also consider the spatial trend of EPE days and the contribution from ARs to EPEs over the selected locations to identify their regional differences.

2. Data and Methods

2.1. ERA5

The fifth generation ECMWF Reanalysis (ERA5) is the latest global reanalysis of the atmosphere created by the ECMWF. It has a horizontal resolution of 0.25° x 0.25° and fields are available every hour (Hersbach et al., 2020). ERA5 shows the best performance in terms of precipitation and other near-surface parameters over Antarctica when compared to other reanalysis (Gossart et al., 2019; Tetzner et al., 2019). Although ERA5 exhibits a slight underestimation (10–15%) in some regions compared to in-situ observations in terms of capturing the frequency of precipitation events, ERA5 is still the best available high-resolution data for a climatological study (1979–2018) of extremes in Antarctica. Surface and upper-level data from the ERA5 reanalysis were employed in this work, including the 10-m wind components, 2-m temperature, integrated water vapour transport components, mean sea level pressure (MSLP), and geopotential height at 500 hPa.

2.2. Identification of EPEs

EPEs over Antarctica were identified using a threshold criteria. In most studies, the threshold value is taken as either a high percentile value (Turner et al., 2019; Welker et al., 2014; Yu et al., 2018) or twice the standard deviation plus the average value (Schlosser, Manning, et al., 2010) of the entire time series. In this study, an EPE day is defined as a precipitation day (precipitation > 0.02 mm) with daily total precipitation greater than the 95th percentile at each location, based on a 40-year climatology. Spatial variability in the 95th percentile values was also analysed to understand the influence of complex orography on precipitation distribution.

By applying the 95th percentile threshold criteria to the time series of precipitation at each grid point for the 40-year study period, variables such as precipitation, 2-m temperature, 10-m wind during EPE days,

157 and the spatial pattern of the total number of EPE days, were found for each latitude-longitude grid point
158 over the region. Daily anomalies in this study were calculated using the mean value for each day for the
159 climatological period 1979-2018 for temperature, MSLP and geopotential height at 500 hPa.
160 We employed a number of techniques, including composite anomaly analysis of MSLP and Empirical
161 Orthogonal Function (EOF) applied to geopotential height anomalies at 500 hPa during EPE days
162 (Grotjahn et al., 2016; Yu et al., 2018) to analyse the synoptic patterns during EPEs. EOF analysis of
163 atmospheric variables during EPEs produces a set of modes that can explain the synoptic pattern on EPE
164 days. We utilised the non-parametric Mann-Kendall (MK) statistical test (Kendall, 1975; Mann, 1945) on
165 the 40-year yearly time series for each grid point to assess the significant trend over the region.

166 **2.3. Directional constancy of wind**

167 Directional constancy (dc) is a technique used to identify the persistent wind direction in a given area. To
168 determine directional constancy during EPE days, we compared wind constancy during these events to
169 directional constancy across the region. Directional constancy is calculated by taking the ratio of the
170 vector-averaged wind speed to the mean wind speed at a height of 10 m (Bromwich, 1989; Ettema et al.,
171 2010). If dc equals 1, the wind direction remains constant, whereas a dc value of zero indicates that the
172 near-surface wind direction is random over time.

$$dc = \frac{(\overline{u}^2 + \overline{v}^2)^{1/2}}{(u^2 + v^2)^{1/2}}$$

173

174 Where u and v are the horizontal components of the 10 m wind.

2.4. AR detection criteria

The AR detection algorithm described by Wille et al. (2021) was used in this study. This algorithm detects the anomalously high (>98th percentile) meridional integrated water vapour transport (vIVT) occurrences every three hours between 37.5˚S and 85˚S. An AR is defined as a continuous, long, narrow band of high IVT values with meridional extent of at least 20 degrees. Although the detection algorithm (Wille et al., 2021) uses both integrated water vapour (IWV) and vIVT for AR detection, this study only uses the vIVT values for AR detection because adding meridional wind speed component reflects the dynamical process that leads to snowfall generation (Wille et al., 2021). To quantify the AR contribution of EPEs, we have used the AR landfall dates detected by this algorithm. We compared these dates with EPE occurrence dates over six selected coastal and inland locations.

3. Results and discussion

3.1. Spatial distribution of EPEs and their characteristics

3.1.1. Precipitation pattern and the complex orography of DML

Figure 1 depicts the characteristics and distribution of precipitation during EPE days compared to the annual mean values, it also shows the elevation contours across DML and the regions with closer contours highlight the steep orographic gradient locations. The annual mean precipitation is high near the coast, but decreases inland (figure 1a). The complex orography of the area has a significant impact on the distribution of precipitation with distinctive features such as ice rises, ice shelves over the coastal areas and the nunataks, mountain ranges, and glacial valleys with steep gradients over the inland region all are being important (Bromwich, 1988; Rotschky et al., 2007; Schlosser et al., 2008). The precipitation

196 distribution has alternate maximum and minimum values occurring near these coastal orographic features
197 with maximum precipitation found on steep east-facing slopes. The ice shelves, especially the ice rise
198 area near 35˚E and 5˚W, show the largest values in the spatial distribution of precipitation. Further inland,
199 the Antarctic ice sheet's elevation rises to around 3700-4000 m above mean sea level and has a dome-
200 shaped form. The lack of moisture and presence of dry katabatic winds lead to much lower precipitation
201 values over these inland regions. Figure 1b shows the annual mean precipitation from EPEs and when
202 comparing to climatological yearly mean precipitation, it shows a similar distribution pattern with a
203 considerable difference in magnitude. This implies that these top 5% precipitation events (EPEs) have a
204 significant role in spatial distribution of total annual precipitation. The precipitation over the continent's
205 interior comes mainly from clear sky precipitation, and the contribution from EPEs is less over these
206 regions due to the infrequent warm air intrusions from ocean regions. The largest 1-day precipitation at
207 each grid point (figure 1c) demonstrates the landfall of these single-day events on the windward side of
208 these orographic features despite the variable orography of the coastal region. EPEs with 70–80 mm/day
209 of precipitation occur close to these orographic features due to the presence of steep slopes that regulate
210 the orographic uplift of warm moist airmass from low latitudes (Welker et al., 2014). The contribution
211 from EPEs (figure 1d) to the total annual precipitation shows that the maximum values are found a little
212 farther southward (around 72˚S). The contribution is more significant near orographic features with steep
213 gradients along the coast than in the vicinity of ice shelves and ice rises. The main cause of this spatial
214 variability between near steep-gradient and near coastal orographic features is the landfall of severe
215 precipitation episodes. Overall, the EPEs thus contribute roughly 35–40% of the total annual precipitation
216 and the maximum impact of EPEs can be seen in the region with steep orographic gradient. The
217 contribution of EPEs to total annual precipitation declines further inland from the coast following the
218 region's orography.

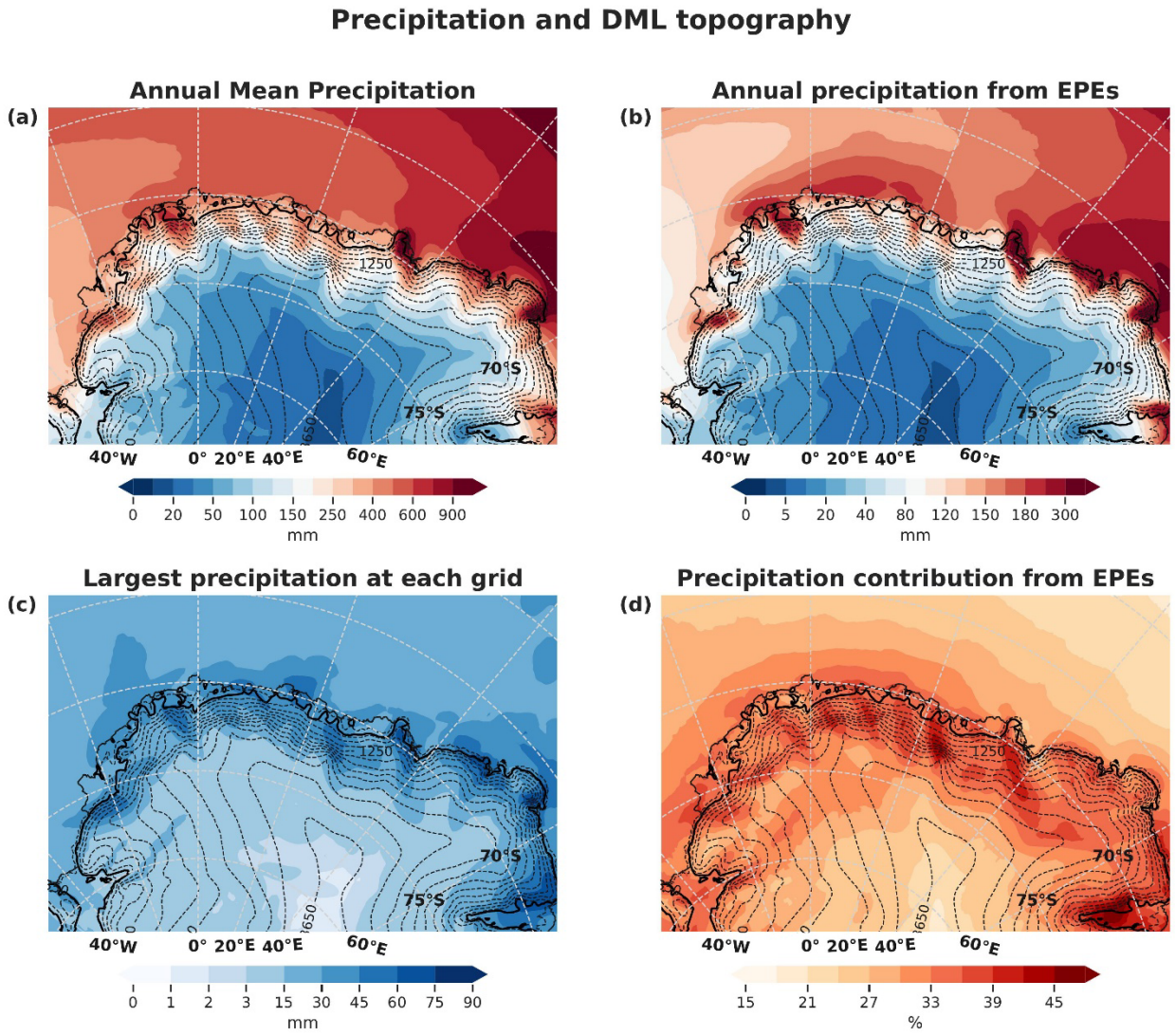

Figure 1. (a) Annual mean precipitation (b) annual mean precipitation from EPEs (c) largest precipitation values at each grid (d) percentage contribution to annual total precipitation from EPEs over DML. All the figures are overlayed by the topography of DML from ERA5 data at 200m contours.

3.1.2. Spatial distribution and variability in the total number of EPE days

To identify the regional differences in the number of high precipitating days and compare its relation to the precipitation distribution from EPEs, we have analysed the total number of EPE days at each grid points over the study region. The spatial distribution of the total number of EPE days (figure 2a) overlaid by elevation contours and wind vectors during EPEs illustrates the interaction of wind flow with the region's complex orography. The spatial variability in the number of EPE days has a pattern with high values over the ocean, coastal, and steep gradient high elevation locations over the interior, and low values on the leeward side of these coastal and inland high orographic regions (leeward side with respect to wind vectors during EPEs). The frequent interaction of easterly to north-easterly winds with these high orographic regions, which often transport sufficient moisture from the ocean during EPEs, can be linked to regional differences in EPE days across these orographic features. Owing to the substantial intrusion and interaction of moisture with these steep gradient regions and the resulting high magnitude precipitation from EPEs, inland regions (around 71˚S to 72˚S) with a steep ice sheet elevation gradient exhibit more EPE days. Due to the lack of these intense precipitation occurrences, the leeward side of these inland high orographic regions have a minimum number of EPE days. Dry downslope winds with northerly to north-easterly directions predominate over these areas during the EPEs. Recent case studies (Gehring et al., 2022; Terpstra et al., 2021) demonstrate the impact of heavy precipitation episodes on the complex terrain of coastal Antarctica and highlighted the importance of the orientation and local processes associated with coastal orography in determining the spatial and temporal distribution of precipitation and snowfall microphysics.

247

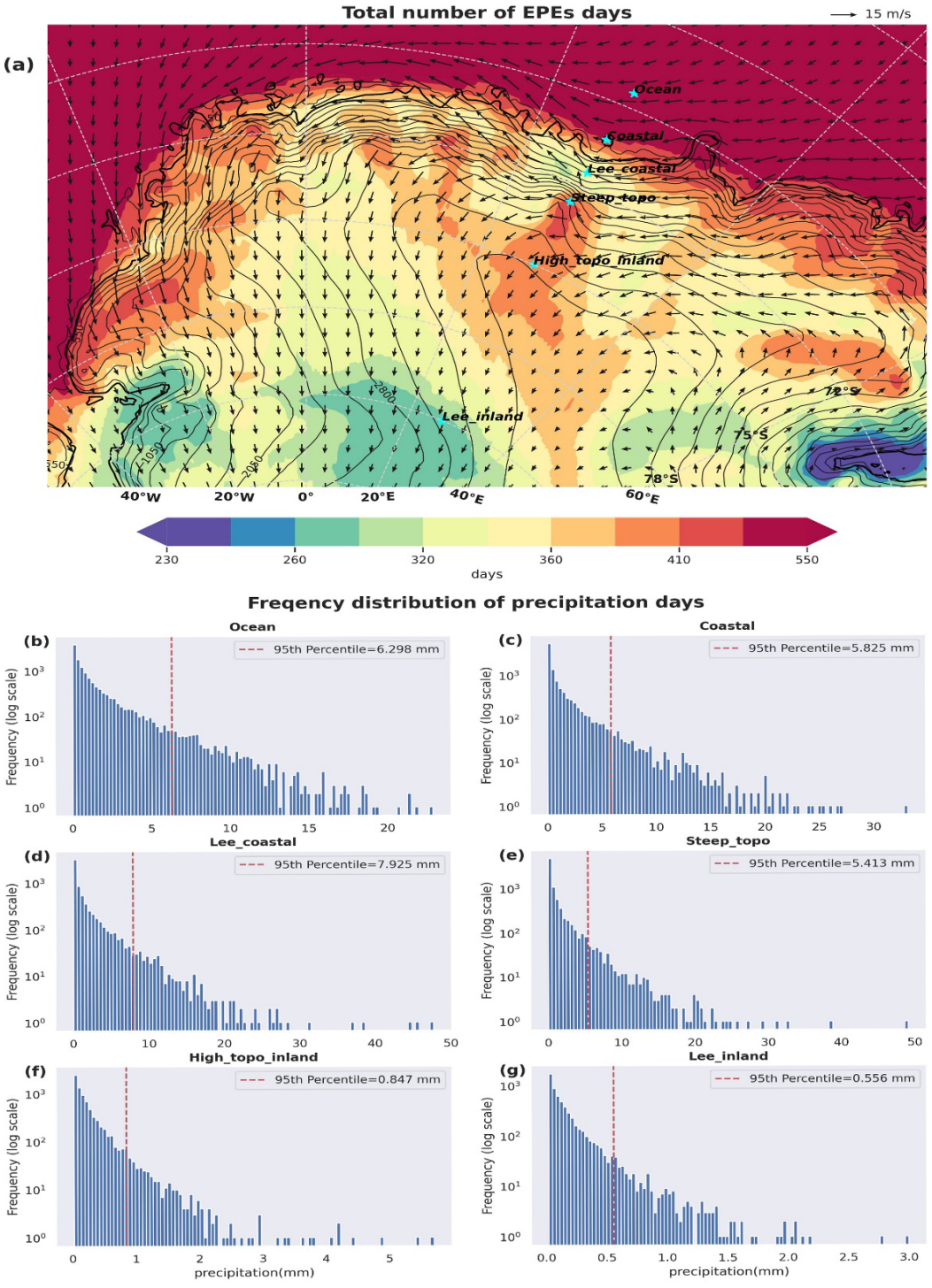

Figure 2. (a) Total number of EPE days for the period 1979-2018 overlayed by the topography of DML and vectors of mean wind during EPEs. Frequency distribution of precipitation days (precipitation value> 0.02mm) in 100 equal

bins of precipitation values at the x-axis and frequency of days in the log scale on the y-axis. Locations selected are (b) Ocean, (c) coastal, (d) lee side of coastal, (e) steep topographic region, (f) high topographic region inland (g) lee side of the high topographic region. The red dotted vertical line shows the value of the EPE threshold (95^{th} percentile).

The frequency distributions of daily precipitation amount from six sites extending from the ocean to the interior with varying numbers of EPE days, is illustrated for a detailed analysis of the range of precipitation values. The distribution is skewed towards the right, with large extreme values found at the tail of the distribution. Locations with a longer tail, or greater separation between the threshold (95th percentile) value and the maximum precipitation, exhibit a more extreme distribution. The ocean and coastal regions (figure 2b, 2c) share a similar 95th percentile value of precipitation. These areas receive frequent precipitation occurrences and a substantial number of days with heavy precipitation. The highest EPE threshold (95^{th} percentile) value among selected points was found on the leeward side of coastal orographic regions (figure 2d), indicating that these areas are prone to frequent events with high precipitation. However, near steep orographic regions (figure 2e), the positively skewed long-tailed precipitation distribution shows a strong extreme nature with a lower threshold value than lee side coastal regions. Although the highest precipitation values in both regions (coastal lee side and near steep orographic regions) are comparable, the 95th percentile values varied based on the presence of extreme values (outliers), the shape of the distribution and the spread of values in the two distributions. A smaller 95th percentile value and more EPE days implies that the precipitation events with large (small) magnitude are more frequent (less frequent) near these steep-orographic regions. High orographic regions inland (figure 2f) also have more EPE days. Maximum precipitation of 5-6 mm per day is seen over these high interior regions, suggesting that moist airmasses reach far inland and cause many EPEs. The lee-sides of these inland high topographic regions (figure 2g) represent the inland precipitation pattern with a small precipitation magnitude and a less extreme distribution. Although clear sky precipitation or

275 'diamond dust' dominates these regions, some precipitation events with a daily precipitation total of 3
276 mm per day occur. The windward slope of coastal orographic and inland steep-gradient regions has a
277 more extreme nature in precipitation distributions, which depends on the wind pattern and interaction of
278 warm moist airmass from the ocean.

279 ### 3.1.3. The meteorological environment during EPEs

280 #### 3.1.3.1. Surface winds

281 The wind speed, directional constancy and comparison with the annual climatology reveals that the
282 direction and speed of the wind during EPEs and the annual mean wind differ noticeably (figure 3). The
283 mean annual wind (figure 3a) is characterised by strong downslope katabatic flow from the high elevation
284 interior, with southerly to south-easterly winds along the coast and particularly over the region 15˚E to
285 45˚E with wind speeds up to 12-15 m/s. Compared to the interior high-elevation region, where wind
286 direction is less consistent, the coastal area has directional consistency close to 0.95 (figure 3b). However,
287 during EPEs (figure 3c, 3d), strong coastal easterlies interact with the complex orography, occurring
288 under remarkably consistent patterns over most of the coastal regions (dc >0.95). Strong coastal easterlies
289 and north-easterlies take the place of katabatic winds during EPEs, causing a warm, moist airmasses to be
290 advected from the ocean. These winds have an average windspeed of >10 m/s, which is considered the
291 threshold value for the blowing snow effect in the Antarctic ice sheet (King & Turner, 1997), especially
292 over the coastal regions. This suggests that blowing snow can be expected during EPEs over the coastal
293 region and that the orography influences wind speed distribution. High wind speeds during these
294 precipitation events can affect post-depositional processes, including erosion, drift, vertical mixing, and
295 blowing snow, all of which can affect the ice core proxy records (Fisher et al., 1985; Karlöf et al., 2005;
296 Münch et al., 2017).

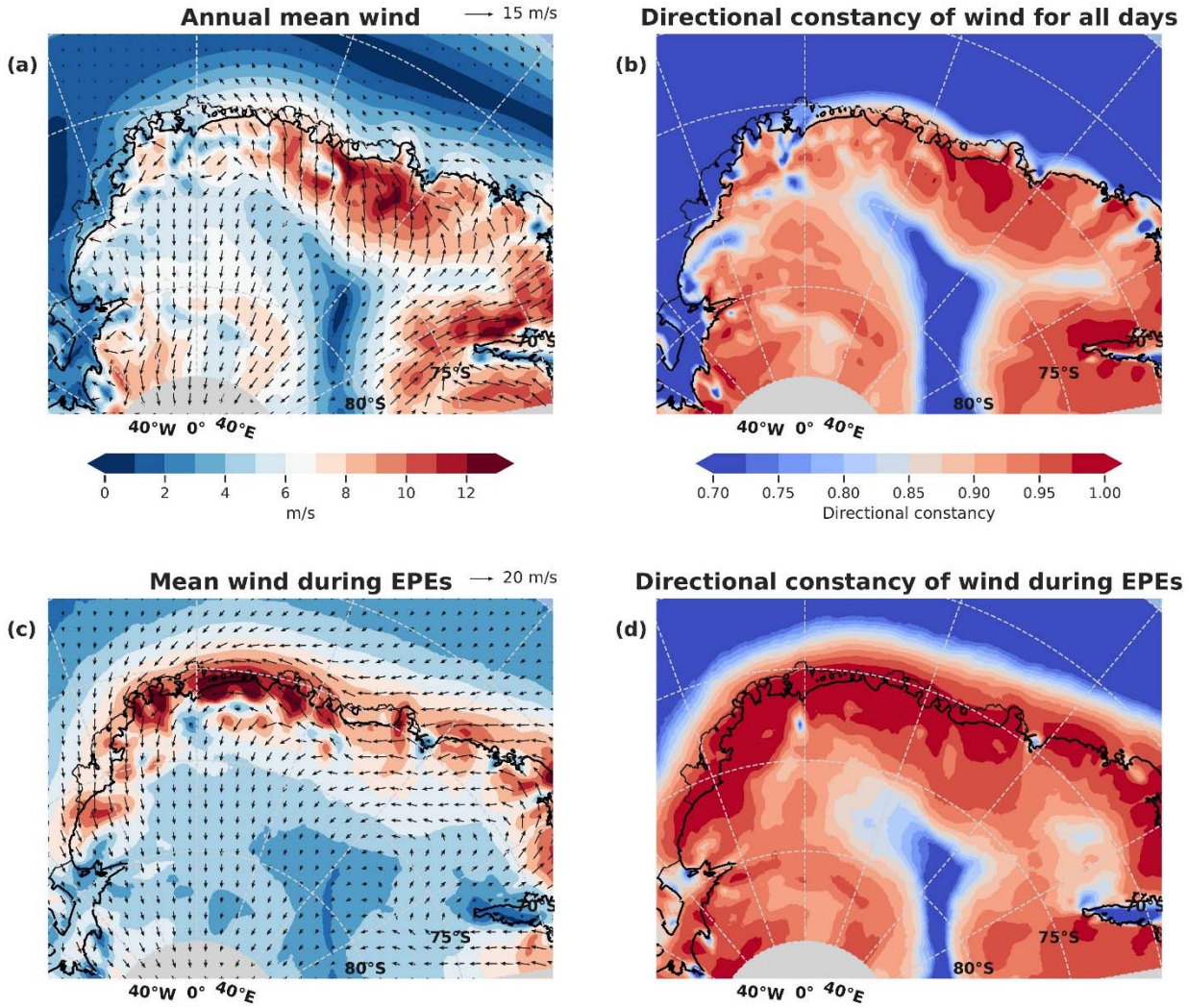

Figure 3. (a) Annual mean wind, (b) directional constancy for all days, (c) mean wind during EPEs, and (d) directional constancy during EPE days.

3.1.3.2. Temperature

The annual mean temperature of the region (figure S1a) is relatively high along the coast and decreases inland. The temperature during EPEs has a similar distribution to the climatological values but with higher values (figure S1b). The average temperature anomaly during EPEs (figure S1c) illustrates that the interior ice sheet areas have high positive anomalies of 10-12 degrees C, particularly across 75˚S-78˚S

close to the Greenwich meridian (0-20E). This region is on the leeward side of the high orographic area that is characterised by dry downslope winds during EPEs. The distribution of maximum temperature anomaly values (figure S1d) is similar to the mean anomaly distribution, with the continental interior having the largest anomalies (23-25 degrees C). Although EPE episodes are less frequent in the interior, they significantly impact the area's temperatures, with a mean anomaly of 10 degrees. Extreme blocking occurrences, warm air advection, cloud cover causing changes in longwave radiation, and strong dry winds contribute to temperature anomalies during EPEs (Hirasawa et al., 2000; Schlosser, Manning, et al., 2010; Servettaz et al., 2020; Turner et al., 2022) particularly in inland areas. When compared to interior sites, the coastal regions experience smaller temperature anomalies during EPEs due to frequent synoptic cyclone landfall and advection of warm airmasses. The high-temperature anomalies during EPEs can cause a significant warm bias in the ice-core records (Jackson et al., 2022; Servettaz et al., 2020), and reconstruction of ice-core isotope data will overestimate reconstructed temperature, if this warm bias is not taken into account (Noone & Simmonds, 1998; Servettaz et al., 2020).

3.2. Temporal variability of EPEs and associated atmospheric processes

3.2.1. Interannual variability of EPEs over selected locations

The spatial variability of the EPE threshold value (95th percentile) is illustrated in figure 4a. The coastal region shows large spatial fluctuations in line with the complex orography of the region. The largest values are found along the ice shelves near 35˚E and 5˚W, and higher values are on the eastward-facing slopes. Precipitation events on the windward and leeward sides of small glacial valleys cause alternate higher and lower 95th percentile values in the coastal area. Inland, the 95th percentile value declines and follows the orography in spatial distribution. The locations with frequent precipitation occurrences have a

higher value in the 95th threshold, which is found to be on the eastward side of coastal orographic features. The six selected locations for temporal analysis are also marked in figure 4a.

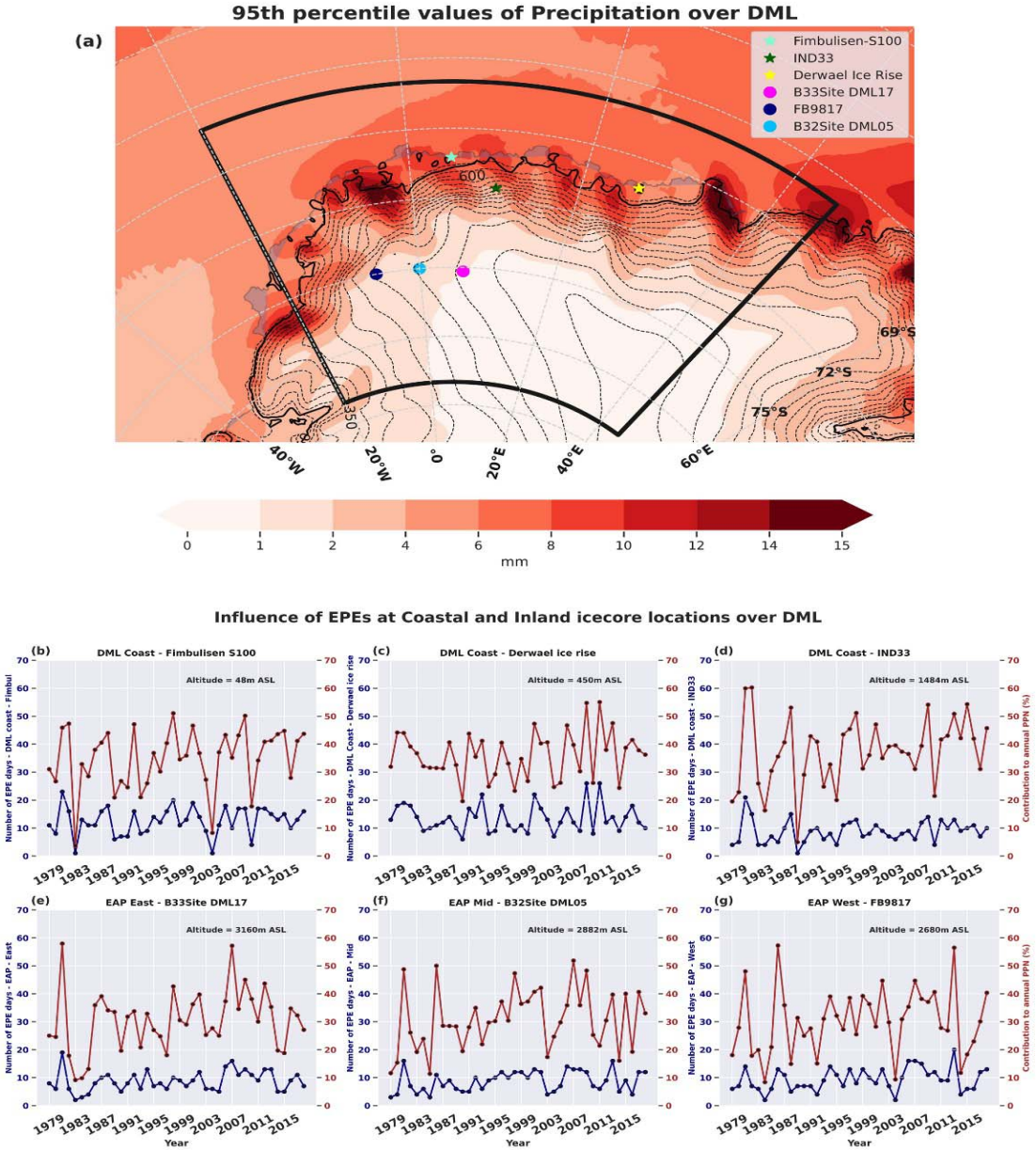

Figure 4. (a) Spatial variability of 95th percentile values with contours of the topography of DML and locations of six locations over DML where three locations from coastal ((b) Fimbulisen S100, (c) Derwael ice rise, (d) IND33) and three from inland ((e) B33Site DML17, (f) B32Site DML05, (g) FB9817). The bold black line over the map

shows the DML area, East Antarctica, temporal variability of the number of EPE days (blue line) and contribution to total annual precipitation (red line) for the period 1979-2018 from these locations.

Ice core location		Latitude, Longitude	Altitude (m)	95th threshold (mm)	Number of EPE days for the 1979-2018 period					AR contribution (%)
					Total	Autumn (MAM)	Winter (JJA)	Spring (SON)	Summer (DJF)	
Coastal	Fimbulisen S100	70.24S,4.8E	48	7.62	503	169	136	121	77	46.5%
	Derwael ice rise	−70.25S,26.34E	450	5.825	539	215	148	107	69	41%
	IND33	71.51S,10.15E	1470	4.534	353	113	106	80	54	56%
Inland	B33Site DML17	75.17S,6.5E	3160	0.9958	350	122	78	75	75	42%
	B32Site DML05	75S,0.01W	2882	1.643	376	136	84	89	67	49.8%
	FB9817	75.0S, 6.5W	2680	1.363	350	117	82	79	72	44%

Table 1. The six ice-core locations were selected for temporal analysis and altitude details as given by Thomas et al. (2017). Features like the 95th percentile value, total number of annual and seasonal EPEs are given in each column. The contribution of atmospheric rivers (AR) in making EPEs at each location in a percentage given in the last column was calculated by comparing the EPE dates with AR landfall dates using the vIVT detection algorithm (Wille et al., 2021).

We selected six locations across the DML region to conduct a temporal analysis of the variability of EPEs throughout coastal and interior locations (Table 1). The selected inland locations lie on the same latitude circle with a significant longitudinal separation. Due to frequent precipitation events in the coastal region, the EPE threshold values and the total number of EPE days decreases from the coast to inland. For all the locations during the study period, the autumn season experienced more EPEs than winter or spring months. However, there is a high interannual variability in EPE occurrence between years. Figure 4 also shows the contribution of precipitation from EPEs to the annual total precipitation and the interannual variability of EPE days for the selected six ice-core locations. In regions close to the ocean (figure 4b,4c,4d), the number of EPE days is relatively high (15–20 days/year) while the number of EPE days is smaller (8–12 days/year) in areas farther inland (figure 4e,4f,4g). Coastal and inland locations have different numbers of EPE days, but on average, the EPEs account for 30%–40% of the total annual precipitation at each location. All areas have a substantial interannual variability in the number of EPE events, significantly influencing the annual total precipitation. The year 1981 had many EPEs at all selected sites, whereas 1983 and 2003 had fewer EPE days. In the following section, we examine the interannual and monthly variability of EPEs and the contributing factors.

3.2.2. **Controlling factors**

The factors controlling the inter-annual variability of EPE days across the coastal and inland stations have been investigated using 500 hpa geopotential height anomalies over a rectangle box (0˚E to 35˚E and 60˚S to 75˚S) to the north of DML. To obtain detailed information about the temporal precipitation distribution and EPE occurrences at the coastal (Fimbulisen S100) and inland (B33Site DML17) stations, we chose years with the largest (year 1981) and smallest (year 1983) number of EPE days for the 40-year period. Figure 5 shows the geopotential height anomalies (area averaged over 0˚E to 35˚E and 60˚S to 75˚S) and daily precipitation values for the coastal and inland station. EPE occurrence was strongly linked with

positive geopotential height anomaly in the selected box, which underlines the importance of strong atmospheric blocking to the north of DML. There were more EPE days at the coastal locations than inland, and these top precipitating days were associated with intense blocking episodes. However, there were some EPE occurrences (9,10 and 23,24 December 1981) along with negative geopotential height anomalies over the box, which indicate the presence of low-pressure systems and the landfall of cyclones over the coastal location. Inland areas, where long-lived strong blocking is necessary for moisture intrusion at high latitudes, show a substantially higher relationship between atmospheric blocking and EPE days. For example, a significant blocking event in mid-January 1981 generated a week-long EPE event (17 to 24 January 1981) across the inland location. The year 1981 was marked by a high frequency of anomalous and episodic atmospheric blocking episodes, which resulted in a larger number of EPE days over both the coastal station (23 EPE days) and that inland (19 EPE days). However, due to less frequent blocking occurrences, the year 1983 experienced fewer number of EPE days, and precipitation occurrences with small precipitation values dominating during that year. Since all blocking events occurred north of DML did not produce significant amounts of precipitation it implies that adequate moisture availability is also a crucial factor for EPE occurrence. The relationship between blocking anticyclones and precipitation generation has been reported in several studies over East Antarctica (Pohl et al., 2021; Schlosser, Manning, et al., 2010; Servettaz et al., 2020; Welker et al., 2014) and our results are consistent with these studies.

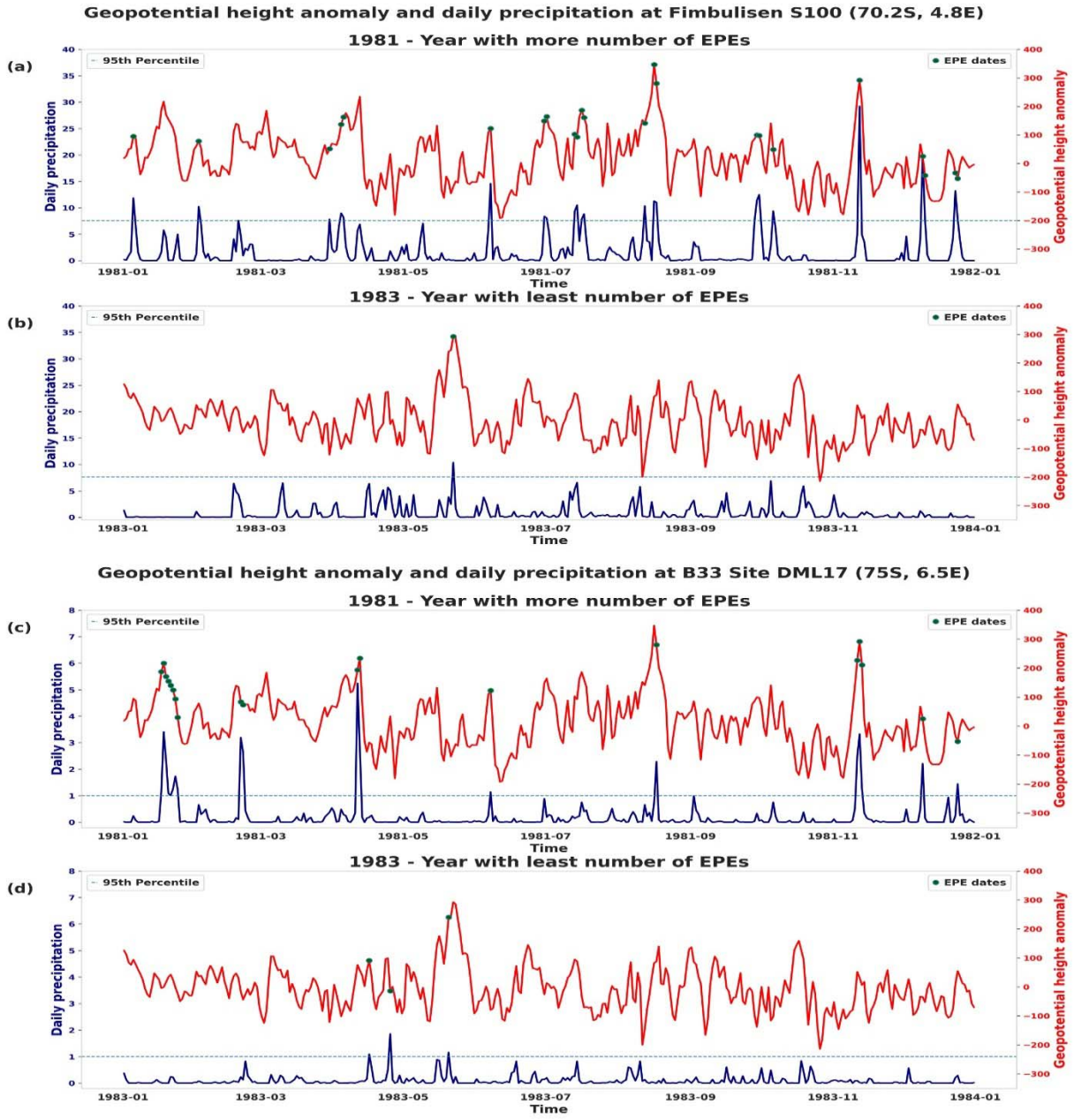

Figure 5. Variability of geopotential height anomaly over a rectangular box north DML (0E to 35E and 60S to 75S) (red line) and daily precipitation values (blue line) with green dots denotes the EPE days with daily precipitation greater than 95th percentile value for a coastal location (Fimbulisen S100) and (a) for the year 1981 - a year with a

386 greater number of EPEs, (b) 1983 – a year with least number of EPEs. (c,d) similar to (a,b) but for an inland location
387 (B33Site DML17)

388 Figure S2 shows each month's total number of EPE days over the 40-year study period. The
389 number of EPE days varied significantly across months for the various sites. All sites show a higher
390 number of EPE days from late autumn to early winter and at the end of the spring season. To investigate
391 this further, we analysed the climatological (1979-2018) monthly MSLP values for each location. The
392 results show a relationship between the weak semi-annual oscillation of MSLP values and the frequency
393 of EPE days. The surface pressure within the circumpolar trough is lower and the trough closer to the
394 continent during equinoctial months and this seasonal change of surface pressure around Antarctica has a
395 crucial effect on the net transfer of air and moisture towards the continent (King & Turner, 1997). The
396 position of the circumpolar trough, modulated by the temperature contrast between mid- and high-
397 latitudes, leads to the semi-annual oscillation in pressure and wind values. The strength of this
398 temperature difference is the largest during the autumnal equinox causing cyclonic activity to peak over
399 the continent (Loon, 1967). The frequency of EPE days during these months is increased by enhanced
400 poleward transport of moist air to higher latitudes during the autumnal equinoctial months. In late winter
401 and summer, there is a similar export of air to lower latitudes (King & Turner, 1997), which results in a
402 decrease in the number of EPE days during those months over the Antarctic. Welker et al. (2014) also
403 observed that the autumn season is when EPE occurrences predominate in DML. Although the number of
404 EPEs has a substantial interannual and seasonal variabilities, no significant relationship was found
405 between the major climate modes (e.g., the Southern Annular Mode (SAM), Southern Oscillation Index
406 (SOI)) and these high precipitation occurrences over the region. This suggests that the SOI and SAM have
407 a relatively small impact on the inter-annual variability of EPEs, with their occurrence primarily
408 determined by regional atmospheric variability.

3.2.3. Atmospheric synoptic conditions during EPEs

To identify the synoptic patterns that occur during EPEs, we used composite anomaly analysis and EOFs of atmospheric variables during EPE days. Figure 6 depicts composites of the MSLP anomaly during EPE episodes at selected locations, including three from the coastal (figure 6a,6c,6e) and three from the interior (figure 6b,6d,6f). A dipole structure of negative (positive) anomalies to the west (east) is present for all chosen locations, with a slight variation in orientation and strength between sites. This implies low pressure to the west and high pressure to the east, with a significant atmospheric block over the region east of the location, which is the typical synoptic pattern during EPEs. The dipole structure is much more evident for coastal locations, where deep low-pressure systems are present to the west of the sites. However, atmospheric blocking to the east is a significant factor for inland locations rather than a few cyclonic intrusions to high latitudes. This dipole structure leads to anomalous northerly and north-easterly winds that carry moisture from mid-latitudes to DML (Welker et al., 2014; Yu et al., 2018). The composite anomaly of geopotential height at 500 hpa (figure S5) also displays similar patterns of this dipole structure of low pressure to the west and high pressure to the east of precipitation location during EPEs.

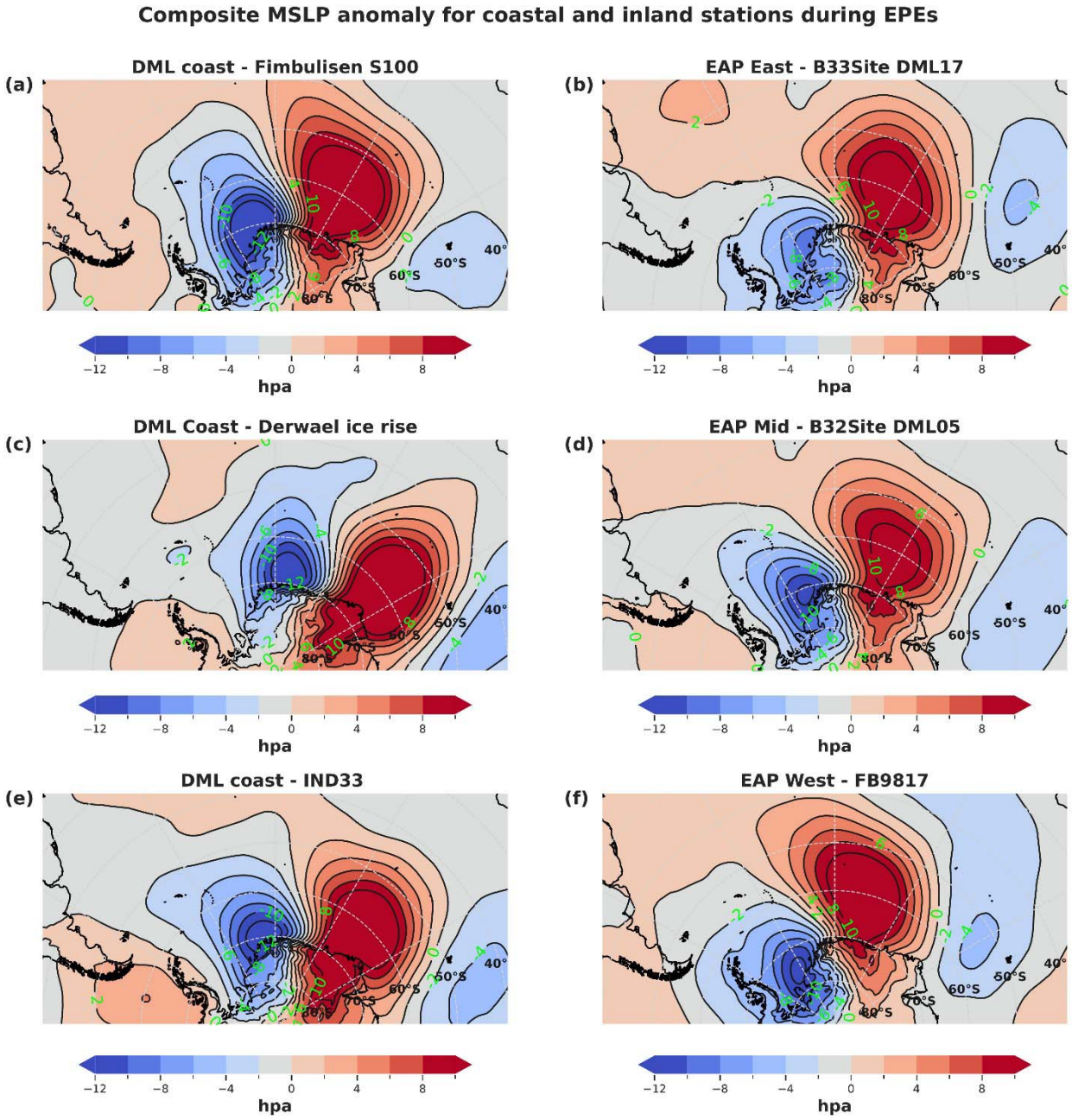

Figure 6. Composite MSLP anomaly during EPE days for six locations. The (a,c,e) is for coastal locations, and the (b,d,f) is for inland locations.

We also used EOF analysis applied to 500-hPa geopotential height (20˚S-90˚S, 90˚W-90˚E) for the 100 largest EPEs over the region, which closely resembles the spatial patterns of the highest

precipitation events. With each row representing a specific location in the figures, the spatial patterns of the first three modes explain more than 40% of the variance exhibited for the coastal area (figure S3) and inland (figure S4) separately. The trough-ridge-trough pattern over the northern part of DML and an eastward shift in this pattern in mode 2 are both apparent in the first two modes, which account for 30% of the variance for the coastal regions. Mode 3 explains about 10% of the variance, describing the eastward-moving low-pressure systems over the south Atlantic Ocean. EPEs over inland areas have a similar trough-ridge-trough pattern strongly correlated with the positive height anomalies north of DML. This highlights the significance of atmospheric blocking for EPE occurrences over the interior locations. Welker et al. (2014) demonstrated that large moisture fluxes towards the interior of DML are associated with a trough-ridge-trough pattern at upper levels and at the surface, a cyclone and blocking high pressure to the west and east of the region, respectively. Our results are consistent with these conclusions, emphasising the importance of strong atmospheric blocking for high precipitation events over inland regions.

3.2.4. **Trends in EPEs and related factors**

The spatial trends in the annual total of extreme precipitation events and related variables are displayed in figure 7. With a magnitude of 0.25 EPE days each year, there is a statistically significant increasing trend (p <0.05) in the number of EPE days to the west of the Greenwich meridian (10˚W to 3˚E) and extending towards the interior around 75-80˚S (figure 7a). In these regions, there is also a significant positive trend in precipitation from EPEs, with a slope of 1-2 mm/year (figure 7b). We analysed the trends in IVT and meridional wind over the Atlantic sector of the Southern Ocean to explain the trends in EPEs (figure 7c, 7d). The results demonstrate a significant (p<0.05) positive trend in IVT values (0.6 kg/ms per year) over the Southern Ocean's Atlantic Sector (over 60˚W to 20˚E), the central moisture transport zone for EPEs in

452 the DML region (figure S6). The meridional wind exhibits a significant negative trend (-0.03 m/s per
453 year), indicating that its more robust southerly component extends to DML, particularly over the 50˚W to
454 5˚W region. Altogether the significant trends in water vapour transport and meridional winds leading to
455 an increased moisture convergence and high precipitating days. Yu et al. (2018) showed that the
456 thermodynamic contribution plays a more significant role in the increasing trend in the occurrence of
457 EPEs. This study also found that the increasing trends in the thermodynamic (IVT) and dynamic
458 (meridional winds) contributions were essential in the positive trend of EPEs over the region. The time
459 series analysis at one of the locations (IND33) shows a significant positive trend ($p<0.05$) in annual
460 precipitation from EPEs but no significant increase in the number of EPE days (figure S7). This suggests
461 that there is an increase in the magnitude of extreme precipitation events in recent decades. In a
462 climatological study of atmospheric rivers over Antarctica, Wille et al. (2021) also found a significant
463 positive trend in AR frequency over DML, particularly in recent decades (2000-2018).

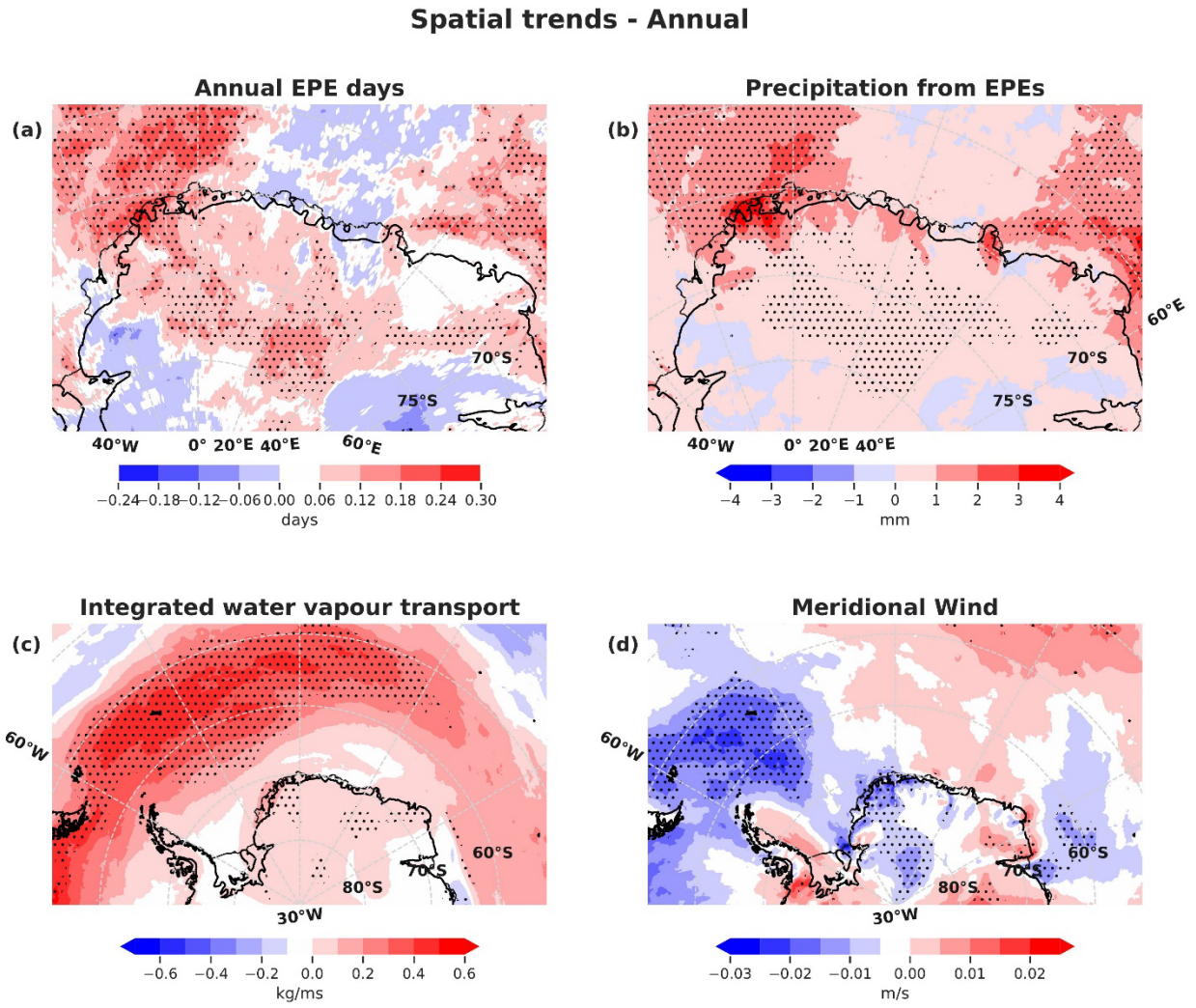

Figure 7. Spatial annual trends in (a) EPE days, (b) precipitation from EPEs, (c) Integrated water vapour transport, and (d) Meridional wind. Locations with statistically significant trends ($p<0.05$) are denoted with dots.

3.2.5. The drivers of EPEs and contribution of atmospheric rivers

The synoptic drivers and moisture transport pathways are identified to gain better understanding of the mechanisms behind EPEs. Welker et al., 2014 demonstrated that the moisture transport (IVT) can be used as a proxy for high precipitation events over coastal and interior DML. With the presence of a synoptic dipole pattern of cyclones in the Weddell Sea and mid-tropospheric ridge to the east of the location

(section 3.2.3), the long-narrow, strong moisture transport through the eastern flank of these low-pressure systems is identified as the major synoptic patterns during EPEs. The occurrence of blocking high pressure systems during EPE days will strengthen the vertically integrated moisture transport (IVT) to DML (Welker et. al., 2014). We analysed the moisture transport pathways during these individual EPEs and found that some of these strong moisture transport events can be identified as atmospheric rivers (AR) as per vIVT detection technique (Wille et al., 2021). For the AR landfall dates at these six different locations, both for coastal and inland, we quantified the percentage of ARs causing EPEs (last column, Table 1). Around 40-50% of high precipitation events were linked to the landfall of ARs, with the largest contribution occurring at IND33 (56%) among coastal sites and B32Site DML05 (50%) among inland areas. The horizontal orientation of this dipole structure creates spatial variability in the AR landfall and generates EPE episodes. An average of 45% of EPE days were associated with AR occurrences in the interior locations with the strong support of a high-pressure ridge to the north of the locations. Wille et al. (2021) also found that 35%-45% of EPEs are associated with ARs over DML, when using the 95th percentile criteria for EPEs. Strong blocking in the eastern portion of the region over the Southern Ocean is a critical requirement for the development of AR and poleward moisture transport (Pohl et al., 2021). In addition, we also analysed the moisture flow patterns for non-AR events (45–50%) separately (not shown). In most cases, the moisture was transported from low latitudes to specifically selected locations as long bands of moisture flow far north of location. These EPE occurrences do not qualify as ARs because the moisture flows that occurred did not meet the length-width and moisture content threshold criteria in the AR detection techniques. Also, we observed some AR landfall dates, with strong moisture content in the atmosphere do not lead to EPEs at DML. Gehring et al. (2022) illustrated that even with strong AR moisture transport, limited precipitation may occur if the flow direction is unfavourable in relation to local orography. Orographic gravity waves and dry downslope winds generated by the interaction between synoptic flow and local orography can cause the sublimation of snowfall below the

cloud base (Gehring et al., 2022). Welker et al. (2014) also suggests a strong link between high precipitation days and moisture flow perpendicular to local orography, which implies the orientation and influence of complex orographic features in giving high precipitation over DML. We used a technique known as self-organizing maps (SOMs – Text S1) that uses IVT during EPE events from a coastal location (IND33) to demonstrate the diversity in moisture transport pathways during EPE occurrences. Figure S6 displays the SOMs of the IVT in a 15-node array with the frequency of occurrence value for each node. The node with a high frequency (node - N9, N10, N11, N14, N15), highlights the AR pattern, whereas the other nodes display moisture transport from a range of directions to the area. Most moisture flux patterns that originate in the Atlantic Ocean come from a region with peak moisture flux values between 30 °S and 50 °S (figure S6), which is in line with the results of Gorodetskaya et al. (2014) and Reijmer & Broeke, (2001). With the synoptic support of low pressure to the west and high pressure to the east of the DML, the moisture flows to the region from various directions from south Atlantic Ocean and causing high magnitude precipitation.

4. Conclusions

We investigated EPEs at high spatial and temporal resolution over the DML region of East Antarctica using ERA5 reanalysis data for the period 1979-2018. We examined their relationship to the complex orography of the region in terms of the spatial distribution of precipitation. Atmospheric synoptic patterns during EPEs were analysed using composite anomalies and EOFs of atmospheric variables, the contributing factors for inter-annual variabilities were also identified.

Our findings show that EPEs, constituting the top 5% of daily precipitation amounts, provided a significant proportion (35%–40%) of the annual total precipitation. The influence of EPEs is dominant along the steep gradient and complex orographic zones, due to the impact of these high precipitation episodes, which contribute 40–45% of the annual total precipitation in just a few days (10–15) per year.

519 Along with the impact on annual precipitation total, EPEs influence surface meteorological variables like
520 surface winds and temperatures. During EPEs, there are persistent and constant strong easterly to
521 northerly winds, and the interaction between these winds and the region's orography has a crucial effect
522 on the spatial distribution of EPE days. When EPEs make landfall, temperatures are anomalously high,
523 significantly impacting inland regions. The synoptic pattern shows that during the majority of EPEs, there
524 are low-pressure anomalies to the west and high-pressure anomalies to the east, with atmospheric
525 blocking to the east of the location being especially important for inland regions. Eastward-moving
526 cyclones and the trough-ridge-trough pattern are crucial in producing EPEs over the region.

527 The temporal variability in the number of EPE days is controlled by atmospheric flow regimes
528 such as atmospheric blocking and changes in the circumpolar trough over the Southern Ocean. As a result
529 of detailed analysis of a number of extreme years, we show the strong relationship between atmospheric
530 blocking and EPE occurrences, especially for inland regions of DML. Over the region, notably central
531 DML, there was an increasing trend in EPE days and EPE-related precipitation. This resulted from the
532 kinetic and thermodynamic changes in the Atlantic section of the Southern Ocean. The increasing trend in
533 integrated water vapor transport and northerly winds has been responsible for the increase in these high-
534 magnitude precipitation events in recent decades, with a significant role for the landfall of strong ARs.
535 This is consistent with the findings of Lenaerts et al. (2013), who identified a positive surface mass
536 balance (SMB) trend across the DML region over the coming decades due to high snowfall anomalies
537 over the region. It is anticipated that this increased snowfall on the East Antarctic ice sheet will greatly
538 mitigate sea level rise in the twenty-first century. By comparing the dates of AR landfall and EPE
539 occurrences from six selected sites spanning the coastal and interior DML, this study determined that 40–
540 50% of EPEs are related to ARs and further supports previous findings about the AR contribution. EPEs
541 have diverse moisture transport pathways, together associated with a dipole structure of low-pressure
542 systems to the west and high pressure to the east.

Since DML is a region for major ice-core based proxy climate studies, the frequency, distribution, and magnitude of EPEs have a significant role in ice-core climate record analysis and interpretation. Our study illustrates anomalous changes in meteorological variables, such as temperature and winds during EPEs, which can cause biases in stable isotope records of ice cores and impact post-depositional features like drifting snow. Detailed case studies of EPE events are required to further understand the influence of orography on the landfall of these events using high-resolution models with a good representation of DML terrain. Increasing trends in EPEs and ARs over DML, which are associated with the changes in atmospheric moisture content and winds, have potential impact on stability of ice shelves over this region in a and warming scenario.

Data availability statement

Copernicus Climate Data Repository provides access to ERA-5 data generated by ECMWF. The source code for the AR detection algorithm discussed in this paper can be accessed at https://doi.org/10.5281/zenodo.4009663.

Acknowledgments

We thank the National Centre for Polar and Ocean Research (NCPOR) for facilities and the Ministry of Earth Sciences (Government of India) for financial support through the project "PACER - Cryosphere and Climate." We also appreciate the support of Pratyush HPC facility at IITM, Pune for computational works. We are grateful to A. Thomas from University of Canterbury, provided valuable advice in SOM analysis. J. D. Wille acknowledges support from the Agence Nationale de la Recherche project, ANR-20-CE01-0013 (ARCA). P. Deb acknowledges the support from the PACER-POP project from NCPOR, NCPOR/2019/PACER-POP/AS-02. Authors also acknowledge HRDG-CSIR for fellowship grant (09/907(0009)/2019-EMR-I) to S.S. This is NCPOR contribution No. xxxxx.

References

Birnbaum, G., Brauner, R., & Ries, H. (2006). Synoptic situations causing high precipitation rates on the Antarctic plateau: Observations from Kohnen Station, Dronning Maud Land. *Antarctic Science*, *18*(2), 279–288. https://doi.org/10.1017/S0954102006000320

Bozkurt, D., Rondanelli, R., Marín, J. C., & Garreaud, R. (2018). Foehn Event Triggered by an Atmospheric River Underlies Record-Setting Temperature Along Continental Antarctica. *Journal of Geophysical Research: Atmospheres*, *123*(8), 3871–3892. https://doi.org/10.1002/2017JD027796

Bromwich, D. H. (1988). Snowfall in high southern latitudes. *Reviews of Geophysics*, *26*(1), 149–168. https://doi.org/10.1029/RG026i001p00149

Bromwich, D. H., Guo, Z., Bai, L., & Chen, Q. (2004). Modeled Antarctic Precipitation. Part I: Spatial and Temporal Variability. *Journal of Climate*, *17*(3), 427–447. https://doi.org/10.1175/1520-0442(2004)017<0427:MAPPIS>2.0.CO;2

Church, J. A., Gregory, J. M., Huybrechts, P., Kuhn, M., Lambeck, K., Nhuan, M. T., Qin, D., & Woodworth, P. L. (2001). *Changes in Sea Level* [Inbook]. , In: J.T Houghton, Y. Ding, D.J. Griggs, M. Noguer, P.J. Van Der Linden, X. Dai, K. Maskell, and C.A. Johnson (Eds.): Climate Change 2001: The Scientific Basis: Contribution of Working Group I to the Third Assessment Report of the Intergovernmental Panel. https://epic.awi.de/id/eprint/4506/

Dalaiden, Q., Goosse, H., Klein, F., Lenaerts, J. T. M., Holloway, M., Sime, L., & Thomas, E. R. (2020). How useful is snow accumulation in reconstructing surface air temperature in Antarctica? A study combining ice core records and climate models. *The Cryosphere*, *14*(4), 1187–1207. https://doi.org/10.5194/tc-14-1187-2020

Fisher, D. A., Reeh, N., & Clausen, H. B. (1985). Stratigraphic Noise in Time Series Derived from Ice Cores. *Annals of Glaciology*, *7*, 76–83. https://doi.org/10.3189/S0260305500005942

590 Gehring, J., Vignon, É., Billault-Roux, A.-C., Ferrone, A., Protat, A., Alexander, S. P., & Berne, A.
591 (2022). Orographic Flow Influence on Precipitation During an Atmospheric River Event at Davis,
592 Antarctica. *Journal of Geophysical Research: Atmospheres*, *127*(2), e2021JD035210.
593 https://doi.org/10.1029/2021JD035210
594 Genthon, C., Krinner, G., & Castebrunet, H. (2009). Antarctic precipitation and climate-change
595 predictions: Horizontal resolution and margin vs plateau issues. *Annals of Glaciology*, *50*(50),
596 55–60. https://doi.org/10.3189/172756409787769681
597 González-Herrero, S., Vasallo, F., Bech, J., Gorodetskaya, I., Elvira, B., & Justel, A. (2023). Extreme
598 precipitation records in Antarctica. *International Journal of Climatology*, *n/a*(n/a).
599 https://doi.org/10.1002/joc.8020
600 Gorodetskaya, I. V., Tsukernik, M., Claes, K., Ralph, M. F., Neff, W. D., & Lipzig, N. P. M. V. (2014).
601 The role of atmospheric rivers in anomalous snow accumulation in East Antarctica. *Geophysical*
602 *Research Letters*, *41*(17), 6199–6206. https://doi.org/10.1002/2014GL060881
603 Gossart, A., Helsen, S., Lenaerts, J. T. M., Broucke, S. V., Lipzig, N. P. M. van, & Souverijns, N. (2019).
604 An Evaluation of Surface Climatology in State-of-the-Art Reanalyses over the Antarctic Ice
605 Sheet. *Journal of Climate*, *32*(20), 6899–6915. https://doi.org/10.1175/JCLI-D-19-0030.1
606 Grotjahn, R., Black, R., Leung, R., Wehner, M. F., Barlow, M., Bosilovich, M., Gershunov, A.,
607 Gutowski, W. J., Gyakum, J. R., Katz, R. W., Lee, Y.-Y., Lim, Y.-K., & Prabhat. (2016). North
608 American extreme temperature events and related large scale meteorological patterns: A review
609 of statistical methods, dynamics, modeling, and trends. *Climate Dynamics*, *46*(3–4), 1151–1184.
610 https://doi.org/10.1007/s00382-015-2638-6
611 Hersbach, H., Bell, B., Berrisford, P., Hirahara, S., Horányi, A., Muñoz-Sabater, J., Nicolas, J., Peubey,
612 C., Radu, R., Schepers, D., Simmons, A., Soci, C., Abdalla, S., Abellan, X., Balsamo, G.,
613 Bechtold, P., Biavati, G., Bidlot, J., Bonavita, M., … Thépaut, J.-N. (2020). The ERA5 global

reanalysis. *Quarterly Journal of the Royal Meteorological Society*, *146*(730), 1999–2049. https://doi.org/10.1002/qj.3803

Hirasawa, N., Nakamura, H., & Yamanouchi, T. (2000). Abrupt changes in meteorological conditions observed at an inland Antarctic Station in association with wintertime blocking. *Geophysical Research Letters*, *27*(13), 1911–1914. https://doi.org/10.1029/1999GL011039

Jackson, S. L., Vance, T. R., Crockart, C., Moy, A., Plummer, C., & Abram, N. J. (2022). Climatology of the Mount Brown South ice core site in East Antarctica: Implications for the interpretation of a water isotope record. *EGUsphere*, 1–36. https://doi.org/10.5194/egusphere-2022-1171

Karlöf, L., Isaksson, E., Winther, J.-G., Gundestrup, N., Meijer, H. A. J., Mulvaney, R., Pourchet, M., Hofstede, C., Lappegard, G., Pettersson, R., Broeke, M. V. D., & Wal, R. S. W. V. D. (2005). Accumulation variability over a small area in east Dronning Maud Land, Antarctica, as determined from shallow firn cores and snow pits: Some implications for ice-core records. *Journal of Glaciology*, *51*(174), 343–352. https://doi.org/10.3189/172756505781829232

Kendall, M. G. (1975). *Rank correlation methods* (4th ed., 2d impression). Griffin.

King, J. C., & Turner, J. (1997). *Antarctic climatology and meteorology*. Cambridge University Press.

Lenaerts, J. T. M., Meijgaard, E. van, Broeke, M. R. van den, Ligtenberg, S. R. M., Horwath, M., & Isaksson, E. (2013). Recent snowfall anomalies in Dronning Maud Land, East Antarctica, in a historical and future climate perspective. *Geophysical Research Letters*, *40*(11), 2684–2688. https://doi.org/10.1002/grl.50559

Lenaerts, J. T. M., & van den Broeke, M. R. (2012). Modeling drifting snow in Antarctica with a regional climate model: 2. Results. *Journal of Geophysical Research: Atmospheres*, *117*(D5). https://doi.org/10.1029/2010JD015419

Lenaerts, J. T. M., van den Broeke, M. R., Déry, S. J., van Meijgaard, E., van de Berg, W. J., Palm, S. P., & Sanz Rodrigo, J. (2012). Modeling drifting snow in Antarctica with a regional climate model:

1. Methods and model evaluation. *Journal of Geophysical Research: Atmospheres*, *117*(D5). https://doi.org/10.1029/2011JD016145

Loon, H. van. (1967). The Half-Yearly Oscillations in Middle and High Southern Latitudes and the Coreless Winter. *Journal of the Atmospheric Sciences*, *24*(5), 472–486. https://doi.org/10.1175/1520-0469(1967)024<0472:THYOIM>2.0.CO;2

Mann, H. B. (1945). Nonparametric Tests Against Trend. *Econometrica*, *13*(3), 245–259. https://doi.org/10.2307/1907187

Markle, B. R., Bertler, N. a. N., Sinclair, K. E., & Sneed, S. B. (2012). Synoptic variability in the Ross Sea region, Antarctica, as seen from back-trajectory modeling and ice core analysis. *Journal of Geophysical Research: Atmospheres*, *117*(D2). https://doi.org/10.1029/2011JD016437

Medley, B., & Thomas, E. R. (2019). Increased snowfall over the Antarctic Ice Sheet mitigated twentieth-century sea-level rise. *Nature Climate Change*, *9*(1), Article 1. https://doi.org/10.1038/s41558-018-0356-x

Münch, T., Kipfstuhl, S., Freitag, J., Meyer, H., & Laepple, T. (2017). Constraints on post-depositional isotope modifications in East Antarctic firn from analysing temporal changes of isotope profiles. *The Cryosphere*, *11*(5), 2175–2188. https://doi.org/10.5194/tc-11-2175-2017

Münch, T., & Laepple, T. (2018). What climate signal is contained in decadal- to centennial-scale isotope variations from Antarctic ice cores? *Climate of the Past*, *14*(12), 2053–2070. https://doi.org/10.5194/cp-14-2053-2018

Noone, D., & Simmonds, I. (1998). Implications for the interpretation of ice-core isotope data from analysis of modelled Antarctic precipitation. *Annals of Glaciology*, *27*, 398–402. https://doi.org/10.3189/1998AoG27-1-398-402

Noone, D., Turner, J., & Mulvaney, R. (1999). Atmospheric signals and characteristics of accumulation in Dronning Maud Land, Antarctica. *Journal of Geophysical Research: Atmospheres*, *104*(D16), 19191–19211. https://doi.org/10.1029/1999JD900376

Pohl, B., Favier, V., Wille, J., Udy, D. G., Vance, T. R., Pergaud, J., Dutrievoz, N., Blanchet, J., Kittel, C., Amory, C., Krinner, G., & Codron, F. (2021). Relationship Between Weather Regimes and Atmospheric Rivers in East Antarctica. *Journal of Geophysical Research: Atmospheres*, *126*(24), e2021JD035294. https://doi.org/10.1029/2021JD035294

Pritchard, H. D., Ligtenberg, S. R. M., Fricker, H. A., Vaughan, D. G., van den Broeke, M. R., & Padman, L. (2012). Antarctic ice-sheet loss driven by basal melting of ice shelves. *Nature*, *484*(7395), 502–505. https://doi.org/10.1038/nature10968

Ralph, F. M., Neiman, P. J., & Wick, G. A. (2004). Satellite and CALJET Aircraft Observations of Atmospheric Rivers over the Eastern North Pacific Ocean during the Winter of 1997/98. *Monthly Weather Review*, *132*(7), 1721–1745. https://doi.org/10.1175/1520-0493(2004)132<1721:SACAOO>2.0.CO;2

Reijmer, C. H., & Broeke, M. R. V. D. (2001). Moisture source of precipitation in Western Dronning Maud Land, Antarctica. *Antarctic Science*, *13*(2), 210–220. https://doi.org/10.1017/S0954102001000293

Reijmer, C. H., & Broeke, M. R. van den. (2003). Temporal and spatial variability of the surface mass balance in Dronning Maud Land, Antarctica, as derived from automatic weather stations. *Journal of Glaciology*, *49*(167), 512–520. https://doi.org/10.3189/172756503781830494

Reijmer, C. H., Van Meijgaard, E., & Van Den Broeke, M. R. (2004). Numerical Studies with a Regional Atmospheric Climate Model Based on Changes in the Roughness Length for Momentum and Heat Over Antarctica. *Boundary-Layer Meteorology*, *111*(2), 313–337. https://doi.org/10.1023/B:BOUN.0000016470.23403.ca

Rignot, E., Mouginot, J., Scheuchl, B., van den Broeke, M., van Wessem, M. J., & Morlighem, M. (2019). Four decades of Antarctic Ice Sheet mass balance from 1979–2017. *Proceedings of the National Academy of Sciences*, *116*(4), 1095–1103. https://doi.org/10.1073/pnas.1812883116

Rotschky, G., Holmlund, P., Isaksson, E., Mulvaney, R., Oerter, H., Broeke, M. R. V. D., & Winther, J.-G. (2007). A new surface accumulation map for western Dronning Maud Land, Antarctica, from interpolation of point measurements. *Journal of Glaciology*, *53*(182), 385–398. https://doi.org/10.3189/002214307783258459

Schlosser, E., Duda, M. G., Powers, J. G., & Manning, K. W. (2008). Precipitation regime of Dronning Maud Land, Antarctica, derived from Antarctic Mesoscale Prediction System (AMPS) archive data. *Journal of Geophysical Research: Atmospheres*, *113*(D24). https://doi.org/10.1029/2008JD009968

Schlosser, E., Manning, K. W., Powers, J. G., Duda, M. G., Birnbaum, G., & Fujita, K. (2010). Characteristics of high-precipitation events in Dronning Maud Land, Antarctica. *Journal of Geophysical Research: Atmospheres*, *115*(D14). https://doi.org/10.1029/2009JD013410

Schlosser, E., Powers, J. G., Duda, M. G., Manning, K. W., Reijmer, C. H., & van den Broeke, M. R. (2010). An extreme precipitation event in Dronning Maud Land, Antarctica: A case study with the Antarctic Mesoscale Prediction System. *Polar Research*, *29*(3), 330–344. https://doi.org/10.3402/polar.v29i3.6072

Schlosser, E., Stenni, B., Valt, M., Cagnati, A., Powers, J. G., Manning, K. W., Raphael, M., & Duda, M. G. (2016). Precipitation and synoptic regime in two extreme years 2009 and 2010 at Dome C, Antarctica – implications for ice core interpretation. *Atmospheric Chemistry and Physics*, *16*(8), 4757–4770. https://doi.org/10.5194/acp-16-4757-2016

Servettaz, A. P. M., Orsi, A. J., Curran, M. A. J., Moy, A. D., Landais, A., Agosta, C., Winton, V. H. L., Touzeau, A., McConnell, J. R., Werner, M., & Baroni, M. (2020). Snowfall and Water Stable

Isotope Variability in East Antarctica Controlled by Warm Synoptic Events. *Journal of Geophysical Research: Atmospheres*, *125*(17), e2020JD032863. https://doi.org/10.1029/2020JD032863

Sinclair, K. E., Bertler, N. a. N., & Trompetter, W. J. (2010). Synoptic controls on precipitation pathways and snow delivery to high-accumulation ice core sites in the Ross Sea region, Antarctica. *Journal of Geophysical Research: Atmospheres*, *115*(D22). https://doi.org/10.1029/2010JD014383

Souverijns, N., Gossart, A., Gorodetskaya, I. V., Lhermitte, S., Mangold, A., Laffineur, Q., Delcloo, A., & van Lipzig, N. P. M. (2018). How does the ice sheet surface mass balance relate to snowfall? Insights from a ground-based precipitation radar in East Antarctica. *The Cryosphere*, *12*(6), 1987–2003. https://doi.org/10.5194/tc-12-1987-2018

Swetha Chittella, S. P., Deb, P., & Melchior van Wessem, J. (2022). Relative Contribution of Atmospheric Drivers to "Extreme" Snowfall Over the Amundsen Sea Embayment. *Geophysical Research Letters*, *49*(16), e2022GL098661. https://doi.org/10.1029/2022GL098661

Terpstra, A., Gorodetskaya, I. V., & Sodemann, H. (2021). Linking Sub-Tropical Evaporation and Extreme Precipitation Over East Antarctica: An Atmospheric River Case Study. *Journal of Geophysical Research: Atmospheres*, *126*(9), e2020JD033617. https://doi.org/10.1029/2020JD033617

Tetzner, D., Thomas, E., & Allen, C. (2019). A Validation of ERA5 Reanalysis Data in the Southern Antarctic Peninsula—Ellsworth Land Region, and Its Implications for Ice Core Studies. *Geosciences*, *9*(7), Article 7. https://doi.org/10.3390/geosciences9070289

Thiery, W., Gorodetskaya, I. V., Bintanja, R., Van Lipzig, N. P. M., Van den Broeke, M. R., Reijmer, C. H., & Kuipers Munneke, P. (2012). Surface and snowdrift sublimation at Princess Elisabeth station, East Antarctica. *The Cryosphere*, *6*(4), 841–857. https://doi.org/10.5194/tc-6-841-2012

731 Thomas, E. R., van Wessem, J. M., Roberts, J., Isaksson, E., Schlosser, E., Fudge, T. J., Vallelonga, P.,
732 Medley, B., Lenaerts, J., Bertler, N., van den Broeke, M. R., Dixon, D. A., Frezzotti, M., Stenni,
733 B., Curran, M., & Ekaykin, A. A. (2017). Regional Antarctic snow accumulation over the past
734 1000 years. *Climate of the Past*, *13*(11), 1491–1513. https://doi.org/10.5194/cp-13-1491-2017
735 Turner, J., Colwell, S. R., & Harangozo, S. (1997). Variability of precipitation over the coastal western
736 Antarctic Peninsula from synoptic observations. *Journal of Geophysical Research: Atmospheres*,
737 *102*(D12), 13999–14007. https://doi.org/10.1029/96JD03359
738 Turner, J., Lachlan-Cope, T. A., Thomas, J. P., & Colwell, S. R. (1995). The synoptic origins of
739 precipitation over the Antarctic Peninsula. *Antarctic Science*, *7*(3), 327–337.
740 https://doi.org/10.1017/S0954102095000447
741 Turner, J., Lu, H., King, J. C., Carpentier, S., Lazzara, M., Phillips, T., & Wille, J. (2022). An Extreme
742 High Temperature Event in Coastal East Antarctica Associated With an Atmospheric River and
743 Record Summer Downslope Winds. *Geophysical Research Letters*, *49*(4), e2021GL097108.
744 https://doi.org/10.1029/2021GL097108
745 Turner, J., Lu, H., King, J., Marshall, G. J., Phillips, T., Bannister, D., & Colwell, S. (2021). Extreme
746 Temperatures in the Antarctic. *Journal of Climate*, *34*(7), 2653–2668.
747 https://doi.org/10.1175/JCLI-D-20-0538.1
748 Turner, J., Phillips, T., Thamban, M., Rahaman, W., Marshall, G. J., Wille, J. D., Favier, V., Winton, V.
749 H. L., Thomas, E., Wang, Z., Broeke, M. van den, Hosking, J. S., & Lachlan-Cope, T. (2019).
750 The Dominant Role of Extreme Precipitation Events in Antarctic Snowfall Variability.
751 *Geophysical Research Letters*, *46*(6), 3502–3511. https://doi.org/10.1029/2018GL081517
752 Welker, C., Martius, O., Froidevaux, P., Reijmer, C. H., & Fischer, H. (2014). A climatological analysis
753 of high-precipitation events in Dronning Maud Land, Antarctica, and associated large-scale

754 atmospheric conditions. *Journal of Geophysical Research: Atmospheres*, *119*(21), 11,932-11,954.
755 https://doi.org/10.1002/2014JD022259
756 Wille, J. D., Favier, V., Dufour, A., Gorodetskaya, I. V., Turner, J., Agosta, C., & Codron, F. (2019).
757 West Antarctic surface melt triggered by atmospheric rivers. *Nature Geoscience*, *12*(11), Article
758 11. https://doi.org/10.1038/s41561-019-0460-1
759 Wille, J. D., Favier, V., Gorodetskaya, I. V., Agosta, C., Kittel, C., Beeman, J. C., Jourdain, N. C.,
760 Lenaerts, J. T. M., & Codron, F. (2021). Antarctic Atmospheric River Climatology and
761 Precipitation Impacts. *Journal of Geophysical Research: Atmospheres*, *126*(8), e2020JD033788.
762 https://doi.org/10.1029/2020JD033788
763 Yu, L., Yang, Q., Vihma, T., Jagovkina, S., Liu, J., Sun, Q., & Li, Y. (2018). Features of Extreme
764 Precipitation at Progress Station, Antarctica. *Journal of Climate*, *31*(22), 9087–9105.
765 https://doi.org/10.1175/JCLI-D-18-0128.1
766 Zhu, Y., & Newell, R. E. (1998). A Proposed Algorithm for Moisture Fluxes from Atmospheric Rivers.
767 *Monthly Weather Review*, *126*(3), 725–735. https://doi.org/10.1175/1520-
768 0493(1998)126<0725:APAFMF>2.0.CO;2
769 Zuhr, A. M., Münch, T., Steen-Larsen, H. C., Hörhold, M., & Laepple, T. (2021). Local-scale deposition
770 of surface snow on the Greenland ice sheet. *The Cryosphere*, *15*(10), 4873–4900.
771 https://doi.org/10.5194/tc-15-4873-2021
772